Cover Page

INTERNATIONAL JOURNAL OF MULTIDISCIPLINARY EDUCATIONAL RESEARCH
ISSN:2277-7881(Print); IMPACT FACTOR :10.16(2026); IC VALUE:5.16; ISI VALUE:2.286
Peer-Peer Reviewed, Refereed & Open Access International Journal - As per UGC Norms
(Fulfilled Suggests Parameters of UGC by IJMER)
Volume:15, Issue:7(2), July 2026
Scopus Review ID: A2B96D3ACF3FEA2A
Article Received: Reviewed: Accepted
Publisher: Sucharitha Publication, India
Online Copy of Article Publication Available: www.ijmer.in

# STRUCTURAL AND MAGNETIC STUDY OF AL-DOPED BARIUM HEXAFERRITE FOR PERMANENT MAGNET IN ELECTRIC VEHICLE APPLICATIONS

**Yaseen Mohd[1], Deepika Sharma[2], Vijay Singh[2] and Indu Sharma[2]**
[1]Center for Green Energy Research, Department of Physics, CPU, Hamirpur, Himachal Pradesh, India
[2]Department of Physics, Himachal Pradesh University, Shimla, 171005, India

**Abstract:**
Al-substituted M-type Ba-hexaferrite $BaFe_{12-x}Al_xO_{19}$ ( x = 0.0, 0.5, 2.5), named "A0", "A1", and "A2", has been prepared via the sol-gel auto-combustion method. The focus is on the study of structural and magnetic properties of M-type hexaferrite. The hexagonal structure of the sample was confirmed via XRD. No traces of impurity peaks have been observed with increasing doping concentration. Morphologies of the samples have been studied using SEM. VSM has been utilised to study the magnetic properties of the material. For the undoped sample, the value of $H_c$ is 4.6 kOe. For x = 2.5, the value increases to 7.56 kOe, i.e., a 64% increment is observed in the value of $H_c$ with 20.8% replacement. This high rise of $H_c$ has made this dopant a potential element to optimize the magnetic properties of M-type hexaferrite for permanent magnets in electric vehicle applications.

**Keywords:** M-type ferrite, Remanence, Coercivity, Permanent Magnet, Electric Vehicle

## Introduction

**Figure 1: Magneto-plumbite structure of M-type BHF**

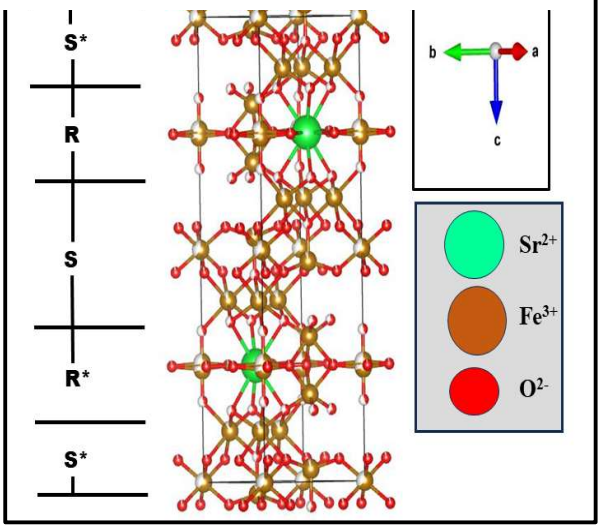


Tourism has emerged as the world's most important economic sector, having a strong impact on global GDP, employment, and international commerce. With this enormous growth, it has sparked serious worries about resource depletion, environmental sustainability, and the effects of climate change. This makes it imperative to comprehend how tourist development might be in line with goals for green growth [1–3]. One way to align tourism with green energy goals is to use low-cost, easily available, non-toxic, and eco-friendly magnetic materials. This original article addresses the primary environmental concerns, i.e., the use of high-cost, rare-earth permanent magnets (PM) in electric vehicles (EVs) [4,5]. In EVs, the motors play a very important role in their operation. In the last few years, scientists have been looking for an alternative to EV motors that does not contain rare-earth elements [6]. Ferrite comes out as the effective solution for that. In terms of the hard magnetic behaviour of ferrite, M-type hexaferrite is the best magnetic material due to its high value of remanence and coercivity as compared to other ferrite materials. To understand the magnetic behaviour of nanoparticles, the study of unit cell structure becomes important as it provides information about the $Fe^{3+}$ sites, responsible for the magnetic behaviour of the nanoparticle.

The $Fe^{3+}$ ions in M-type HF are the main cause of the hard magnetic properties of ferrite. The structure of M-type hexaferrite is shown in Figure 1. The $Fe^{3+}$ ions exist in five crystal lattice sites within the M-type HF structure, such as three octahedral sites (2a, 12k, and $4f_2$), one tetrahedral site ($4f_1$), and one trigonal bipyramidal site (2b). Although the spins of the $4f_2$ and $4f_1$ sites are directed oppositely, the spins of the 12k, 2a, and 2b sites in the oriented magnetic phase of BHF are aligned in parallel [7]. Microstructure and magnetic characteristics of these materials may be altered by replacing some of these $Fe^{3+}$ ions in the hexagonal structure with various divalent and trivalent cations.

Cover Page

INTERNATIONAL JOURNAL OF MULTIDISCIPLINARY EDUCATIONAL RESEARCH
ISSN:2277-7881(Print); IMPACT FACTOR :10.16(2026); IC VALUE:5.16; ISI VALUE:2.286
Peer-Peer Reviewed, Refereed & Open Access International Journal - As per UGC Norms
(Fulfilled Suggests Parameters of UGC by IJMER)
Volume:15, Issue:7(2), July 2026
Scopus Review ID: A2B96D3ACF3FEA2A
Article Received: Reviewed: Accepted
Publisher: Sucharitha Publication, India
Online Copy of Article Publication Available: www.ijmer.in

The paper studies the Al-doped M-type BHF, i.e., $BaFe_{12-x}Al_xO_{19}$, where x = 0.0, 0.5, and 2.5. The samples have been named A0, A1, and A2, respectively. The diamagnetic $Al^{3+}$ ion has been used to increase the $H_c$ of the material.

Experimental Details

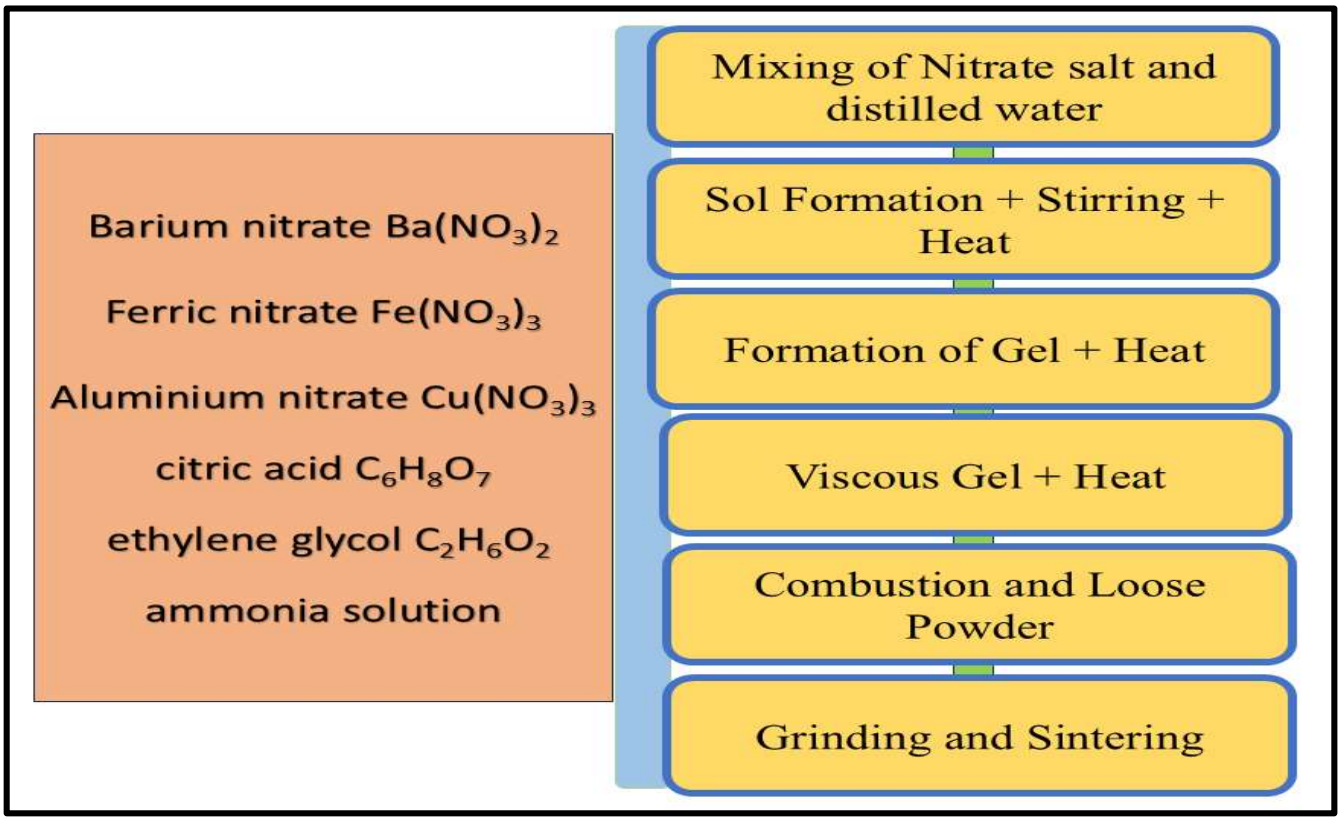


**Figure 2: Flow chart for the Sol-gel Auto-Combustion Method**

Researchers have used different types of methods, such as ball-milling [8,9], laser evaporation [10], co-precipitation [11,12], sol-gel [13,14], citrate precursor [15]and sol-gel auto-combustion [16], etc., for the formation of ferrite magnetic nanoparticles (MNP). This series, i.e., Al-doped M-type Ba-ferrite, $BaAl_xFe_{12-x}O_{19}$ (x = 0.0, 0.5, 2.5) (A0, A1 and A2), has been prepared via the sol-gel auto-combustion route (as shown in Figure 2). Barium nitrate Ba $(NO_3)_2$, Ferric nitrate nonahydrate $Fe(NO_3)_3 \cdot 9H_2O$ (99-101%, Purity), Aluminium nitrate $Al(NO_3)_3 \cdot xH_2O$ (98.5%, Purity), Anhydrous citric acid $C_6H_8O_7$, ethylene glycol $C_2H_6O_2$, and ammonia solution obtained from Central Drug House (P) Ltd are used in the preparations [17]. Figure 2 shows the systematic diagram for the preparation of nanoparticles via this process.

There are several sol-gel techniques, each with its own advantages and suitability for specific ferrite formation. Researchers use sol-gel spectral approaches to choose the best way to synthesize ferrites with specific properties. Compared with other synthesis processes, the sol-gel methodology offers several advantages. It makes it possible to have precise stoichiometric control, ensuring that the final product has the desired chemical composition [18]. Additionally, Smaller particle sizes can be produced as tiny powders using the sol-gel technique, and this is essential for uses where increased reactivity and surface area are required [19]. However, one disadvantage of the Sol-gel approach is the agglomeration of particles, which can limit performance. Various strategies, such as the use of capping agents and optimized drying procedures, can be employed to minimize agglomeration and improve the overall quality of the synthesized ferrites. Despite this challenge, High-quality ferrite materials with specific characteristics may still be produced using the sol-gel process.

Cover Page

INTERNATIONAL JOURNAL OF MULTIDISCIPLINARY EDUCATIONAL RESEARCH
ISSN:2277-7881(Print); IMPACT FACTOR :10.16(2026); IC VALUE:5.16; ISI VALUE:2.286
Peer-Peer Reviewed, Refereed & Open Access International Journal - As per UGC Norms
(Fulfilled Suggests Parameters of UGC by IJMER)
Volume:15, Issue:7(2), July 2026
Scopus Review ID: A2B96D3ACF3FEA2A
Article Received: Reviewed: Accepted
Publisher: Sucharitha Publication, India
Online Copy of Article Publication Available: www.ijmer.in

The sol-gel technique is based on the use of metal nitrates as precursors and citrate as fuel, which react in solution to form a gel [20]. Shortly thereafter, this gel is heated, causing ferrite NPs to form. The sol-gel approach guarantees uniformity and excellent purity in the produced materials, making it appropriate for applications requiring high-quality ferrites [21]. Furthermore, the sol-gel approach can minimize process steps and the time spent creating powder, simplifying the production process and increasing efficiency [18]. By carefully controlling the amounts of precursors and reaction conditions, researchers can alter the properties of the produced ferrites to satisfy specific application needs.

Results and Discussion:

**3.1. XRD Analysis:**

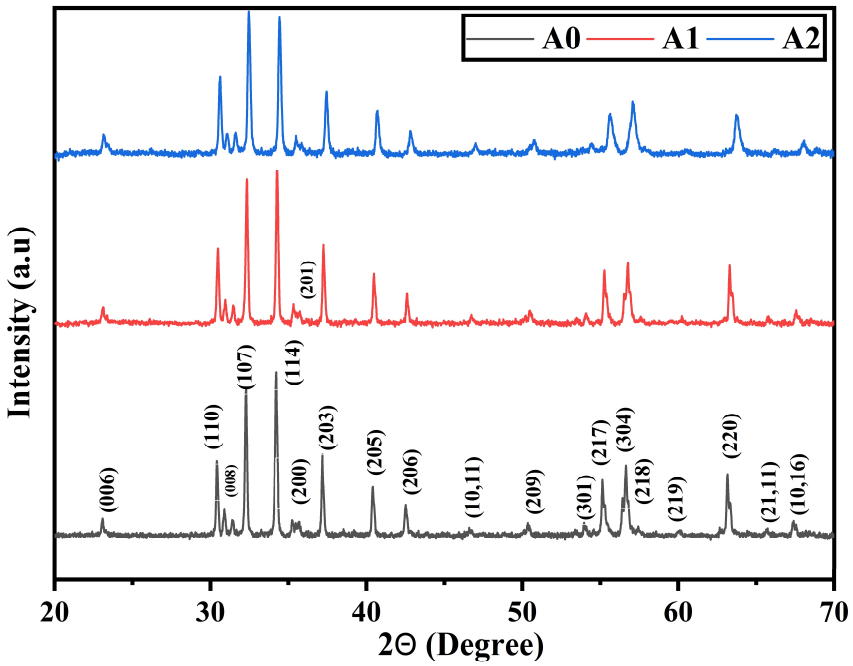


**Figure 3: XRD structure of Pure and Al-doped M-type Ba hexaferrite, named "A0", "A1," and "A2"**

The XRD patterns of aluminium-doped $BaFe_{12-x}Al_xO_{19}$ ( x = 0.0, 0.5, 2.5), named A0, A1, and A2, were analysed by means of an XRD device at room temperature (RT). The XRD graphs of all synthesized samples of Ba- containing M-type hexagonal ferrites prepared via the sol-gel auto-combustion method are shown in Figure 3. The XRD patterns of the single-phase hexagonal $BaFe_{12-x}Al_xO_{19}$ ( x = 0.0, 0.5, 2.5) matched with the ICDD card number – 01-080-1198 [22]. From the XRD spectrum, it is clear that the maximum intensity of the reflection was obtained for A0, A1, and A2 at the values of 2Θ = 34.2 º, 34.27º, and 34.41º, respectively, which are in good agreement with the literature data [23]. It is clear from Figure 3 that no traces of the impurity phase have been found. The complete diffusion of $Al^{3+}$ into the BHF crystal is indicated by the absence of any secondary phase. The structural phase remains the same for all dopant concentrations, but there were minor changes with respect to the relative intensity and shifting of peaks resulting from the Al substitution.

The value of the lattice parameters is shown in Table 1. Figure 4 also shows the variation of structural parameters with dopant concentration. The values of the lattice constants "a" and "c" are calculated using the formula given in Equation 1 as [24]:

Cover Page

INTERNATIONAL JOURNAL OF MULTIDISCIPLINARY EDUCATIONAL RESEARCH
ISSN:2277-7881(Print); IMPACT FACTOR :10.16(2026); IC VALUE:5.16; ISI VALUE:2.286
Peer-Peer Reviewed, Refereed & Open Access International Journal - As per UGC Norms
(Fulfilled Suggests Parameters of UGC by IJMER)
Volume:15, Issue:7(2), July 2026
Scopus Review ID: A2B96D3ACF3FEA2A
Article Received: Reviewed: Accepted
Publisher: Sucharitha Publication, India
Online Copy of Article Publication Available: www.ijmer.in

$$\frac{1}{d_{hkl}^2} = \frac{4}{3}\left(\frac{h^2+hk+k^2}{a^2}\right) + \frac{l^2}{c^2} \qquad \ldots\ldots\ldots (1)$$

Where $d_{hkl}$ is the interplanar spacing and h, k, l are the Miller indices of the planes. For the undoped sample, i.e., pure BHF ($BaFe_{12}O_{19}$), the values "a" and "c" are 5.882 Å and 23.01 Å, respectively.

As the $Al^{3+}$ dopant concentration increases, the value of lattice parameters decreases. For A1, the values of "a" and "c" are 5.868 Å and 22.98 Å, and for A2, the values are 5.830 Å and 23.03 Å, respectively. These results are consistent with the previous study on Al-doped M-type HF [25]. This change can be attributed to the fact that the ionic radius of $Al^{3+}$ (0.535 Å) is smaller than that of $Fe^{3+}$ (0.645 Å) [26].

Grain size determination D (hkl) was done using Scherrer's formula [27].

$$D = \frac{0.9\,\lambda}{\beta COS\theta} \qquad \ldots\ldots\ldots\ldots (2)$$

Where D denotes the average crystallite size, λ denotes the X-ray wavelength, β stands for full width at half maximum (FWHM), and Θ is the Bragg's angle. For A0-A2, the value of crystallite sizes changes from 33.30 nm to 29.66 nm. The graphical variation of crystallite size and strain has been shown in Figure 5. The value of the c/a ratio for pure and Al-doped BHF falls between 3.911 and 3.946. The value of the c/a ratio less than 3.98 confirms the formation of the hexagonal phase in M-type HF [28].

**Table 1: The value of lattice parameter, cell volume, c/a ratio, crystallite size, Dislocation density, and Strain for Pure and Al-doped M-type Ba-hexaferrite.**

| Sample | a (Å) | c (Å) | $V_{cell}$ (Å$^3$) | c/a | Crystallite size (nm) | Dislocation Density (1/nm$^2$) | Strain (ε) |
|---|---|---|---|---|---|---|---|
| **A0** | 5.882 | 23.01 | 689.47 | 3.911 | 33.30 | 0.001 | 0.062 |
| **A1** | 5.868 | 22.98 | 685.74 | 3.917 | 33.05 | 0.009 | 0.0009 |
| **A2** | 5.830 | 23.03 | 679.60 | 3.946 | 29.66 | 0.2630 | 0.0011 |

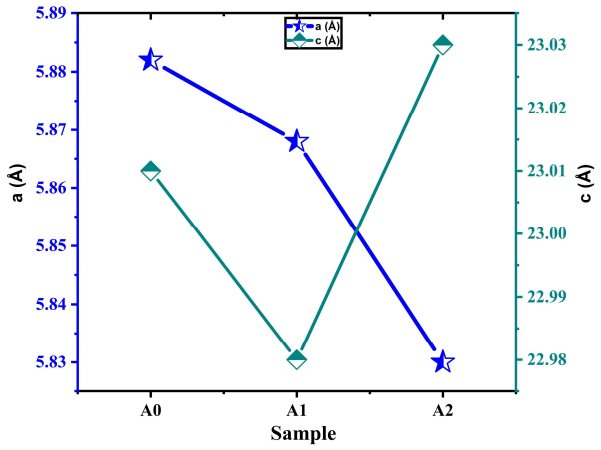


**Figure 4: Variation in the value of the lattice parameter with varying dopant concentration of Al in M-type BHF**

Cover Page

INTERNATIONAL JOURNAL OF MULTIDISCIPLINARY EDUCATIONAL RESEARCH
ISSN:2277-7881(Print); IMPACT FACTOR :10.16(2026); IC VALUE:5.16; ISI VALUE:2.286
Peer-Peer Reviewed, Refereed & Open Access International Journal - As per UGC Norms
(Fulfilled Suggests Parameters of UGC by IJMER)
Volume:15, Issue:7(2), July 2026
Scopus Review ID: A2B96D3ACF3FEA2A
Article Received: Reviewed: Accepted
Publisher: Sucharitha Publication, India
Online Copy of Article Publication Available: www.ijmer.in

**Figure 5: Variation in the value of the crystallite size and strain with varying dopant concentration of Al in M-type BHF**

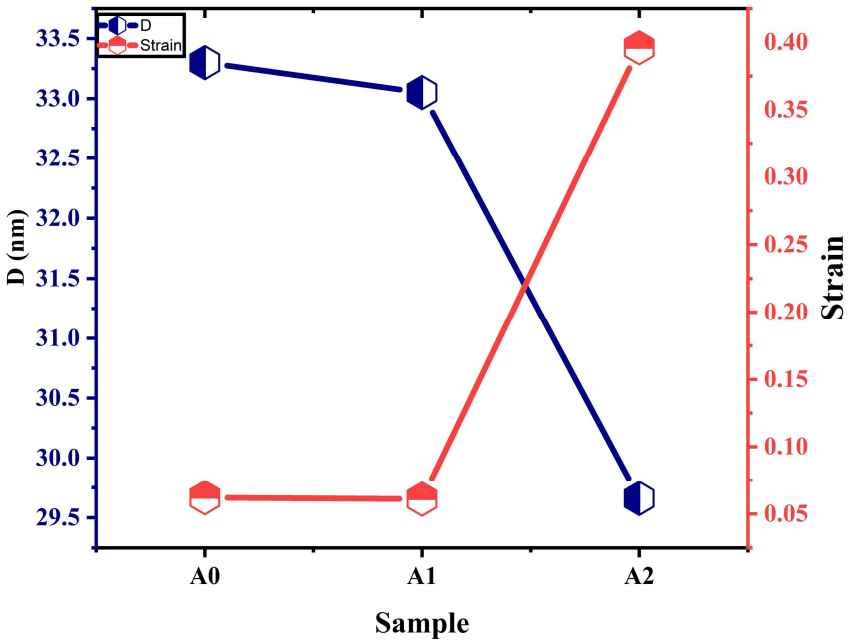


The dislocation density of the material is used to measure the crystallinity of the material. With the increase in crystallinity, the dislocation density value decreases, while with a decrease in crystallinity, the dislocation density value increases [29]. Equation 3 is used to compute its value, which is given by:

$$\delta = \frac{1}{D^2} \qquad \text{.....(3)}$$

The values of dislocation density for A0, A1, and A2 are 0.001, 0.0009, and 0.2630, respectively.

The formula [30] was used to determine the strain (**ε**) caused by doping, as given below in equation 4:

$$\varepsilon = \frac{\beta COS\Theta}{4} \qquad \text{.....(4)}$$

The value of the calculated strain is given in Table 1.

### 3.2. SEM Analysis:

**Figure 6: FE-SEM Micrographs of Al-doped M-type Ba-hexaferrite**

Cover Page

INTERNATIONAL JOURNAL OF MULTIDISCIPLINARY EDUCATIONAL RESEARCH
ISSN:2277-7881(Print); IMPACT FACTOR :10.16(2026); IC VALUE:5.16; ISI VALUE:2.286
Peer-Peer Reviewed, Refereed & Open Access International Journal - As per UGC Norms
(Fulfilled Suggests Parameters of UGC by IJMER)
Volume:15, Issue:7(2), July 2026
Scopus Review ID: A2B96D3ACF3FEA2A
Article Received: Reviewed: Accepted
Publisher: Sucharitha Publication, India
Online Copy of Article Publication Available: www.ijmer.in

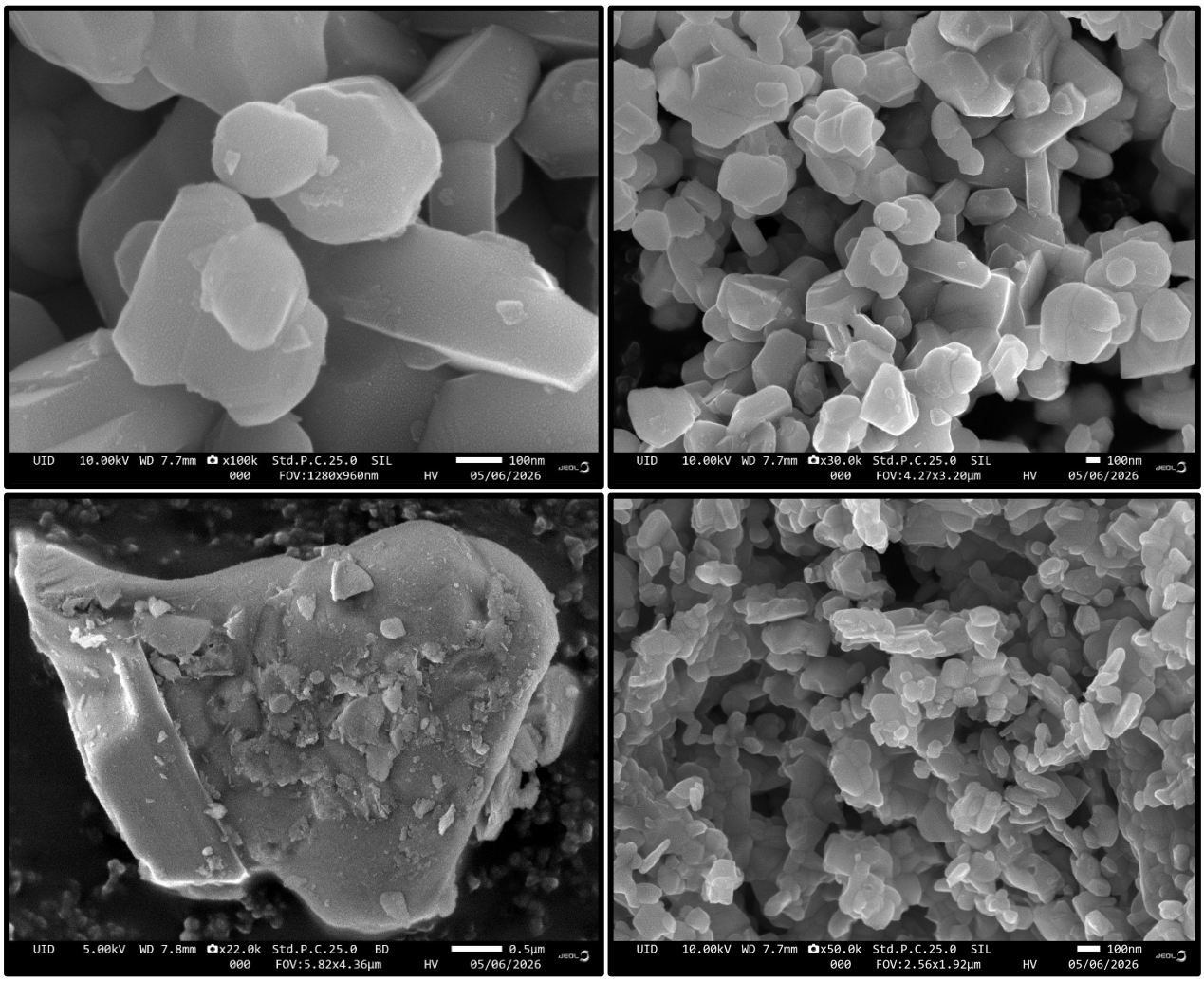


Figure 6 shows FE-SEM images of Al-doped BHF ($BaFe_{12-x}Al_xO_{19}$). The images show non-uniformity of the particles, where some grains exhibit square, cubic, or rectangular shapes while some of them are in hexagonal shapes. SEM images clearly depict that the grains are porous, which does not allow the passage of charge through the grain boundaries. This will affect the electrical properties and polarization in the same way as porosity influences the magnetic properties [31].

Cover Page

INTERNATIONAL JOURNAL OF MULTIDISCIPLINARY EDUCATIONAL RESEARCH
ISSN:2277-7881(Print); IMPACT FACTOR :10.16(2026); IC VALUE:5.16; ISI VALUE:2.286
Peer-Peer Reviewed, Refereed & Open Access International Journal - As per UGC Norms
(Fulfilled Suggests Parameters of UGC by IJMER)
Volume:15, Issue:7(2), July 2026
Scopus Review ID: A2B96D3ACF3FEA2A
Article Received: Reviewed: Accepted
Publisher: Sucharitha Publication, India
Online Copy of Article Publication Available: www.ijmer.in

### 3.3. Magnetic study:

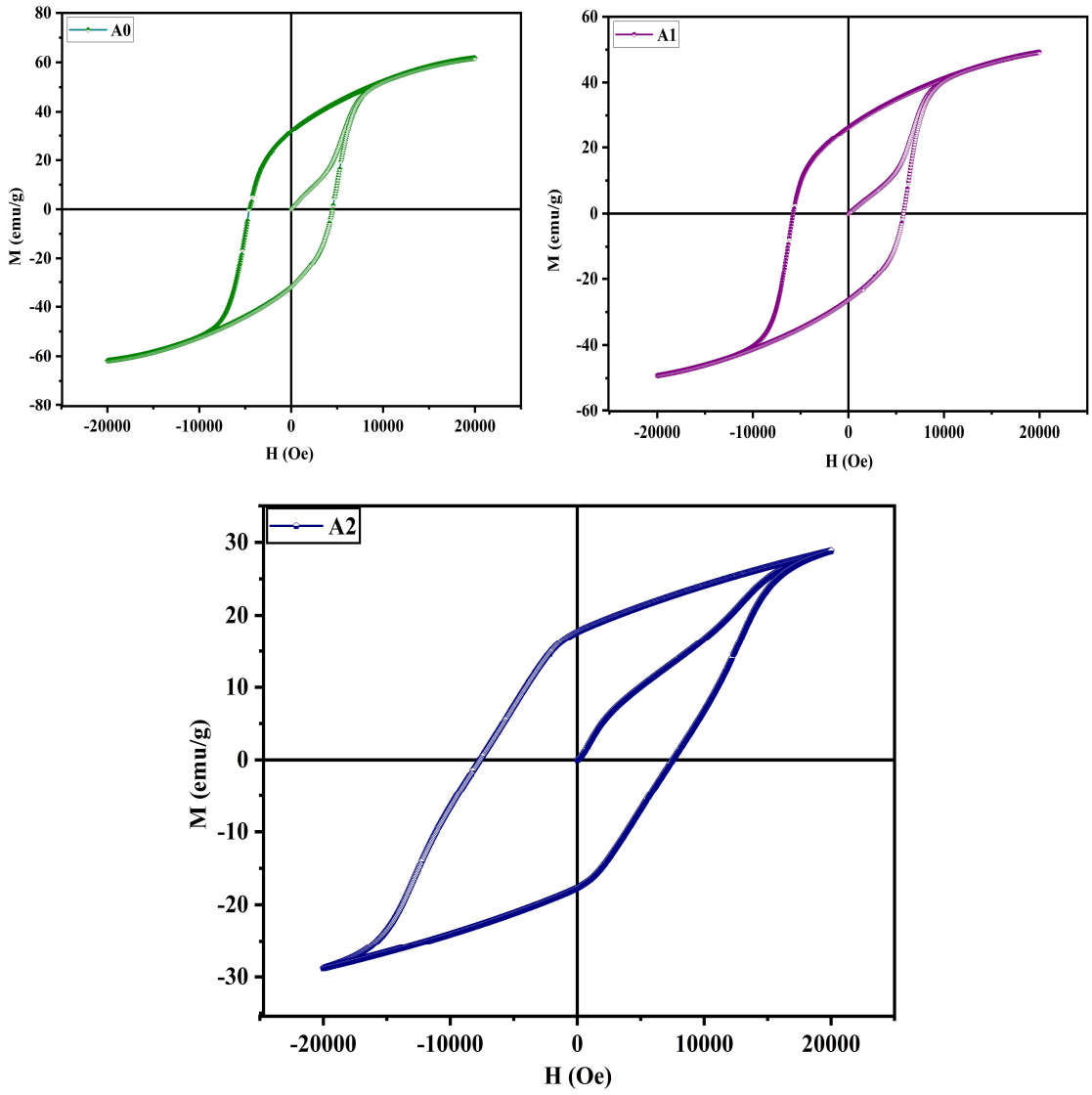


**Figure 7: Hysteresis loop for Pure and Al-doped M-type BHF, named "A0", "A1", and "A2", respectively.**

Cover Page

INTERNATIONAL JOURNAL OF MULTIDISCIPLINARY EDUCATIONAL RESEARCH
ISSN:2277-7881(Print); IMPACT FACTOR :10.16(2026); IC VALUE:5.16; ISI VALUE:2.286
Peer-Peer Reviewed, Refereed & Open Access International Journal - As per UGC Norms
(Fulfilled Suggests Parameters of UGC by IJMER)
Volume:15, Issue:7(2), July 2026
Scopus Review ID: A2B96D3ACF3FEA2A
Article Received: Reviewed: Accepted
Publisher: Sucharitha Publication, India
Online Copy of Article Publication Available: www.ijmer.in

**Table 2: The values of $M_s$ (emu/g), $M_r$ (emu/g), $H_c$ (kOe), $M_r / M_s$ for pure and Al-doped M-type Ba-hexaferrite**

| Composition (x) | $M_s$ (emu/g) | $M_r$ (emu/g) | $H_c$ (kOe) | $M_r / M_s$ |
|---|---|---|---|---|
| **A0** | 61.78 | 31.70 | 4.6 | 0.513 |
| **A1** | 49.2 | 26.41 | 5.78 | 0.536 |
| **A2** | 28.83 | 17.78 | 7.56 | 0.616 |

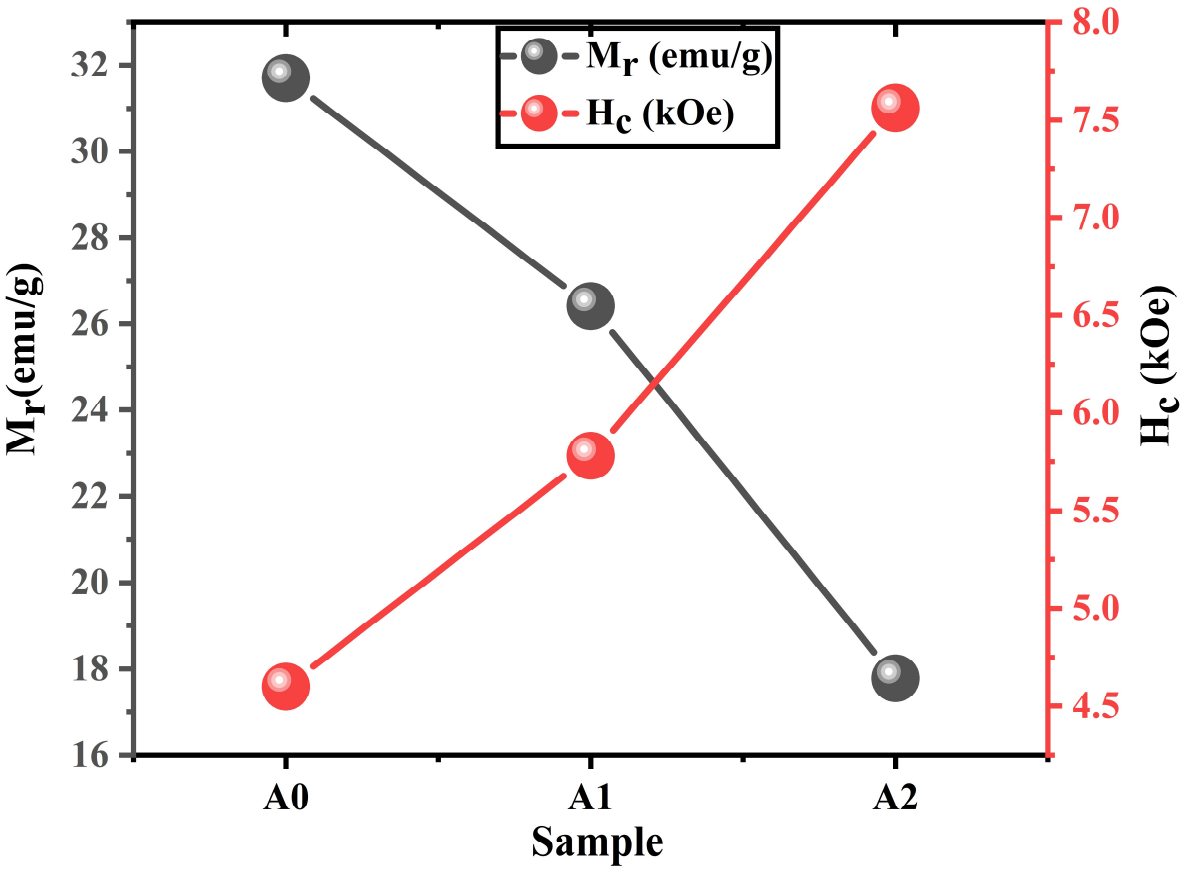


**Figure 8: Variation in the values of $M_r$ (emu/g) and $H_c$ (kOe) with Al doping in M-type Ba-Hexaferrite**

Cover Page

INTERNATIONAL JOURNAL OF MULTIDISCIPLINARY EDUCATIONAL RESEARCH
ISSN:2277-7881(Print); IMPACT FACTOR :10.16(2026); IC VALUE:5.16; ISI VALUE:2.286
Peer-Peer Reviewed, Refereed & Open Access International Journal - As per UGC Norms
(Fulfilled Suggests Parameters of UGC by IJMER)
Volume:15, Issue:7(2), July 2026
Scopus Review ID: A2B96D3ACF3FEA2A
Article Received: Reviewed: Accepted
Publisher: Sucharitha Publication, India
Online Copy of Article Publication Available: www.ijmer.in

The magnetic properties of Pure and Al-doped BHF, $BaFe_{12-x}Al_xO_{19}$ ( x = 0.0, 0.5, 2.5), named A0, A1, and A2, powdered material were examined using VSM at RT (300 K), with an applied magnetic field of 20 kOe. The hysteresis loop derived for A0, A1, and A2 is shown in Figure 7. The hard ferromagnetic behaviour with large $H_c$ is confirmed by the typical behaviour of all magnetic isotherms and the existence of a strong, detectable hysteresis loop. This loop is in good agreement with the previously reported hard ferromagnetic nature of HF [32,33].

The calculated values of $M_s$, $M_r$, and $H_c$ for Al-doped BHF with different dopant concentrations, under sample names A0, A1, and A2, are presented in Table 2, while their graphical changes are depicted in Figure 8. From Figure 7, it is clear that the substitution of $Al^{3+}$ ions has a significant impact on the magnetic behaviour of BHF. The values of $M_s$, $M_r$, and $H_c$ for undoped BHF, i.e., for A0, are 61.78 emu/g, 31.70 emu/g, and 4.6 kOe, respectively. As the amount of dopant concentration increases to x = 0.5 and x = 2.5, the value of $H_c$ significantly improves, while a decrease in the values of $M_s$ and $M_r$ has been observed.

For samples "A1" and "A2", the value of $M_s$ reduces to 49.2 emu/g and 28.83 emu/g, while $M_r$ reduces to 26.41 emu/g and 17.78 emu/g, respectively. The decrement in the magnetisation of BHF is due to the replacement of $Al^{3+}$ ions on different sites in the hexagonal structure of ferrite. The $Fe^{3+}$ ions are unevenly distributed in five non-equivalent sublattices: One is tetrahedral ($4f_1$), one is trigonal bipyramidal (2b), and the other three are octahedral (2a, 12k, and $4f_2$). These five sites are responsible for the magnetic moment in M-type HF [33]. The 12k (6 sites), 2a (1 site), and 2b (1 site) are in the spin-up state, while $4f_1$ (2 sites) and $4f_2$ (2 sites) are in the spin-down state. Uncompensated upward spins are the cause of the total magnetic moment, or 20 $\mu_B$. Site occupancy refinement has revealed that $Al^{3+}$ ions predominantly occupy the 2a and 12k sites, whereas a small fraction occupies the $4f_2$ (octahedral) site. The 2b site, i.e., trigonal bipyramidal, exhibits a higher substitution value when x >2; the $4f_1$ site possesses a small proportion of < 5 % [34]. The diamagnetic $Al^{3+}$ ion replaces the $Fe^{3+}$ ion (magnetic moment = 5 $\mu_B$) from the sites with spin-up orientation, mostly from 12k sites [26]. This will lead to a reduction in $M_s$ and $M_r$ of the synthesised compounds. As non-magnetic $Al^{3+}$ ions replace $Fe^{3+}$ ions, the super-exchange interactions between $Fe^{3+}$-O-$Fe^{3+}$ also diminish [35,36]. The non-collinear spin arrangements are created as a result of this reduction in exchange interactions. As a result of this, the randomly oriented spin arrangement of the surface layer with respect to the c-axis is formed. The net magnetisation of the material is further reduced by the coupling of canted surface spins with the c-axis-aligned core spin [26].

On the other hand, $H_c$ represents the coercivity of the ferrimagnetic material. The value is the magnitude of the magnetic field needed to bring the sample's magnetisation down to zero once it has attained saturation. For the undoped sample, the value of $H_c$ is 4.6 kOe. For x= 0.5, the value of $H_c$ increases to 5.78 kOe. With just 4.16 % of replacement of $Al^{3+}$ ions via $Fe^{3+}$, the percental increment in the value of $H_c$ is 25%. Simultaneously, in sample "A2", 64% of the increment is observed in the value of $H_c$ with 20.8 % of replacement. The particle size and magneto-crystalline anisotropy play a major role in the effect of $H_c$ on Al doping. Luo et al. explained that the single-domain limit of nanoparticles increases as the level of Al dopant rises, and thus the grain would exhibit the SD behaviour [26].

The creation of an SD impeded the domain-wall movement, which results in the rise of $H_c$. However, the role of the domain wall in defining $H_c$ is difficult to determine since defects can pin and nucleate domain barriers [26]. Additionally, when $Al^{3+}$ is added as a replacement for $Fe^{3+}$, the $H_c$ rises as predicted from $H_c = \alpha(2K/M_S)$ [37], where K is the magneto-crystalline anisotropy, and $M_s$ is the magnetic saturation. This formula indicates that the $H_c$ of the material increases as saturation magnetization decreases. This improvement in $H_c$ behaviour is achieved with less than 0.7% Al substitution, demonstrating the effectiveness of aluminium doping in improving the hard magnetic properties of the material. This suggests that Al can serve as an efficient substitute for enhancing the coercivity, thereby optimizing the magnetic performance for permanent magnet applications. Such a doping strategy offers a potential pathway towards developing a cost-effective and optimized ferrite-based material for high-performance applications, particularly in permanent magnetic technologies in electrical vehicle applications.

Cover Page

INTERNATIONAL JOURNAL OF MULTIDISCIPLINARY EDUCATIONAL RESEARCH
ISSN:2277-7881(Print); IMPACT FACTOR :10.16(2026); IC VALUE:5.16; ISI VALUE:2.286
Peer-Peer Reviewed, Refereed & Open Access International Journal - As per UGC Norms
(Fulfilled Suggests Parameters of UGC by IJMER)
Volume:15, Issue:7(2), July 2026
Scopus Review ID: A2B96D3ACF3FEA2A
Article Received: Reviewed: Accepted
Publisher: Sucharitha Publication, India
Online Copy of Article Publication Available: www.ijmer.in

**Conclusion:**

Al-doped M-type Ba-hexaferrite, $BaFe_{12-x}Al_xO_{19}$ ( x = 0.0, 0.5, 2.5), named A0, A1, and A2, has been successfully synthesised via the sol-gel auto-combustion method. XRD analysis was carried out for structure identification. The peaks of the XRD pattern are very similar to those of the standard pattern for the P63/mmc group. The value of the lattice parameter decreases with increasing dopant concentration. The crystallite size also reduces with dopant concentration and lies in the range of 29.66 nm to 33.30 nm. This change can be attributed to the fact that the ionic radius of $Al^{3+}$ (0.535 Å) is smaller than that of $Fe^{3+}$ (0.645 Å). The morphology of the particle has been confirmed via SEM. The study of magnetic properties reveals a 64% increment in the $H_c$ of the sample. The $H_c$ of the samples has been improved from 4.6 kOe to 7.56 kOe, but $M_r$ reduces from 31.70 emu/g for A0 to 17.78 emu/g for A2, respectively. This improvement in $H_c$ makes the $Al^{3+}$ dopant a potential candidate for the improvement in $H_c$ of the material. The material has the potential to be utilised as a permanent magnet material for electric vehicle applications.

**References :**

[1] A. Mahanta, R. Samal, N.C. Sahu, Harnessing Renewable Energy to Advance Sustainable Tourism and Green Growth: A G20 Countries' Perspective, Energy RESEARCH LETTERS 7 (2026). https://doi.org/10.46557/001C.156401.

[2] H. Rasool, S. Maqbool, Md. Tarique, The relationship between tourism and economic growth among BRICS countries: a panel cointegration analysis, Future Business Journal 2020 7:1 7 (2021) 1-. https://doi.org/10.1186/S43093-020-00048-3.

[3] W. You, Y. Zhang, C.C. Lee, Climate Risk, Economic Stability, and Tourism: A Cross-Sectionally Dependent Heterogeneous Panel Causality Analysis, Energy RESEARCH LETTERS 2 (2021). https://doi.org/10.46557/001C.25723.

[4] S.S. Rangarajan, C.K. Shiva, E.R. Collins, T. Senjyu, Electric Vehicle Motors Free of Rare-Earth Elements—An Overview, Machines 2025, Vol. 13, 13 (2025). https://doi.org/10.3390/MACHINES13080702.

[5] I. Mohammed, J. Mohammed, A.K. Srivastava, Recent Progress in Hexagonal Ferrites Based Composites for Microwave Absorption, Crystal Research and Technology 58 (2023) 2200200. https://doi.org/10.1002/CRAT.202200200;PAGE:STRING:ARTICLE/CHAPTER.

[6] J.R. Riba, C. López-Torres, L. Romeral, A. Garcia, Rare-earth-free propulsion motors for electric vehicles: A technology review, Renewable and Sustainable Energy Reviews 57 (2016) 367–379. https://doi.org/10.1016/J.RSER.2015.12.121.

[7] W. Abbas, I. Ahmad, M. Kanwal, G. Murtaza, I. Ali, M. Azhar Khan, M.N. Akhtar, M. Ahmad, Structural and magnetic behavior of Pr-substituted M-type hexagonal ferrites synthesized by sol–gel autocombustion for a variety of applications, J. Magn. Magn. Mater. 374 (2015) 187–191. https://doi.org/10.1016/J.JMMM.2014.08.029.

[8] M.H. Mahmoud, A.M. Hassan, A.E.A.A. Said, T.A. Taha, Structural, magnetic, and catalytic studies of microwave-combustion/ball-mill synthesized zinc ferrite nanoparticles, Inorg. Chem. Commun. 144 (2022) 109932. https://doi.org/10.1016/J.INOCHE.2022.109932.

[9] S.M. Yasin, Superparamagnetic Ni0.5Zn0.5Fe2O4 nanoparticles prepared by ball-milling, Applied Physics A 2023 129:10 129 (2023) 672-. https://doi.org/10.1007/S00339-023-06954-X.

[10] Synthesis of magnetic nanoparticles by laser ablation of strontium ferrite under water and their characterization by optically detected magnetophoresi ... - Journal of Materials Chemistry C (RSC Publishing) DOI:10.1039/D1TC04796E, (n.d.).

[11] A. Saremi, S.M. Mirkazemi, A. Sazvar, H. Rezaie, Controlling magnetic and surface properties of cobalt ferrite nanoparticles: A comparison of co-precipitation and solvothermal synthesis methods, Solid State Sci. 148 (2024) 107432. https://doi.org/10.1016/J.SOLIDSTATESCIENCES.2023.107432.

Cover Page

INTERNATIONAL JOURNAL OF MULTIDISCIPLINARY EDUCATIONAL RESEARCH
ISSN:2277-7881(Print); IMPACT FACTOR :10.16(2026); IC VALUE:5.16; ISI VALUE:2.286
Peer-Peer Reviewed, Refereed & Open Access International Journal - As per UGC Norms
(Fulfilled Suggests Parameters of UGC by IJMER)
Volume:15, Issue:7(2), July 2026
Scopus Review ID: A2B96D3ACF3FEA2A
Article Received: Reviewed: Accepted
Publisher: Sucharitha Publication, India
Online Copy of Article Publication Available: www.ijmer.in

[12] Moatoshi, S.K. Sah, S.D. Kaushik, J.P. Borah, Structural and magnetic properties of M-type hexaferrite nanoparticles: A comparative analysis of BaFe12O19 and SrFe12O19 synthesized via chemical co-precipitation, Ceram. Int. 50 (2024) 22599–22607. https://doi.org/10.1016/J.CERAMINT.2024.03.361.

[13] X. Wang, B. Wang, S. Wei, Y. Wang, Y. Liang, Effect of sintering temperature on the microstructure, magnetic, and microwave absorption properties of M-type barium ferrite nanoparticles prepared by sol–gel method, Journal of Materials Science: Materials in Electronics 2023 34:12 34 (2023) 1045-. https://doi.org/10.1007/S10854-023-10400-2.

[14] A.I. Borhan, A.R. Iordan, D. Ghercă, M.N. Palamaru, Ferrite nanoparticles by sol–gel method, Ferrite Nanostructured Magnetic Materials: Technologies and Applications (2023) 103–119. https://doi.org/10.1016/B978-0-12-823717-5.00047-4.

[15] I. Sharma, M. Vineet Sharma, P. Sharma, A REVIEW ON SYNTHESIS AND CHARACTERIZATION OF MNZN FERRITE NANOPARTICLES VIA CITRATE PRECURSOR METHOD, Peer Reviewed and Refereed Journal (2022) 11.

[16] D. Sharma, R. Duglet, V. Singh, Y. Mohd, A. Dogra, M. Singh, Tailoring magnetic parameters of M-type hexaferrites via Nd-Al doping for rare-earth-free permanent magnet in EV's, Phys. Lett. A 579 (2026) 131517. https://doi.org/10.1016/J.PHYSLETA.2026.131517.

[17] A. Manhas, K. Batoo, M.S.-J. of A. and Compounds, undefined 2018, Magnetic and Mössbauer investigations of soft Co2Z-type hexa nano ferrites, Elsevier (n.d.). https://www.sciencedirect.com/science/article/pii/S092583881832615X (accessed January 17, 2023).

[18] D. Bokov, A. Turki Jalil, S. Chupradit, W. Suksatan, M. Javed Ansari, I.H. Shewael, G.H. Valiev, E. Kianfar, Nanomaterial by Sol-Gel Method: Synthesis and Application, Advances in Materials Science and Engineering 2021 (2021) 5102014. https://doi.org/10.1155/2021/5102014.

[19] S. Fayazzadeh, M. Khodaei, Salt-assisted combustion synthesis of cobalt ferrite nanoparticles; magnetic properties and cation distribution measurement by XRD analysis, Journal of Ultrafine Grained and Nanostructured Materials 52 (2019) 69–77. https://doi.org/10.22059/JUFGNSM.2019.01.07.

[20] M.K.A. Kar, F. Manteghi, M. Ghahari, M.K.A. Kar, F. Manteghi, M. Ghahari, Microwave assisted sol-gel auto-combustion synthesis of NiCuFe2O4 nanoparticles using citric acid as an organic chelating agent: structural and optical studies, (2015) c005. https://doi.org/10.3390/ECSOC-19-C005.

[21] S.C. Tolani, A.R. Golhar, K.G. Rewatkar, A review of morphological, structural behaviour and technological applications of ferrites, AIP Conf. Proc. 2104 (2019). https://doi.org/10.1063/1.5100459/888717.

[22] S. Gulbadan, S.R. Ejaz, A.H. Nizamani, I. Shakir, P.O. Agboola, M.N. Akhtar, M.F. Warsi, M.A. Khan, Structural elucidation and dielectric behavior evaluation of sol-gel synthesized Co–Al co-substituted M-type hexaferrite materials, Ceram. Int. 46 (2020) 4914–4923. https://doi.org/10.1016/J.CERAMINT.2019.10.228.

[23] Y. Yang, F. Wang, D. Huang, J. Shao, J. Tang, K.M. Ur Rehman, Z. Wu, Influence of Sn-Mg co-substitution on the microstructural and magnetic characteristics of M-type SrCaLa hexagonal ferrites, J. Magn. Magn. Mater. 452 (2018) 100–107. https://doi.org/10.1016/J.JMMM.2017.12.047.

[24] C.T. Tchouank Tekou, B. Thiodjio Sendja, A. Alshoaibi, J. Sharma, J. Mohammed, S. Sharma, C.A. Njeumen, F.I. Ezema, A.K. Srivastava, Crystal Structure Refinement, Bond Length, Raman Spectroscopy and Magnetic Properties of Al3+- and Ce3+-Codoped M-Type Barium Hexagonal Ferrite, (2024). https://doi.org/10.2139/SSRN.4944459.

[25] H. Luo, B.K. Rai, S.R. Mishra, J.P. Liu, H. Luo, B.K. Rai, S.R. Mishra, V. V Nguyen, Physical and magnetic properties of highly aluminum doped strontium ferrite nanoparticles prepared by auto-combustion route, Journal of Magnetism and Magnetic Materials 324 (2013) 2602–2608. https://doi.org/10.1016/j.jmmm.2012.02.106.

[26] H. Luo, B.K. Rai, S.R. Mishra, V. V. Nguyen, J.P. Liu, Physical and magnetic properties of highly aluminum doped strontium ferrite nanoparticles prepared by auto-combustion route, J. Magn. Magn. Mater. 324 (2012) 2602–2608. https://doi.org/10.1016/j.jmmm.2012.02.106.

[27] B.D. Cullity, Elements of X-ray Diffraction,

Cover Page

INTERNATIONAL JOURNAL OF MULTIDISCIPLINARY EDUCATIONAL RESEARCH
ISSN:2277-7881(Print); IMPACT FACTOR :10.16(2026); IC VALUE:5.16; ISI VALUE:2.286
Peer-Peer Reviewed, Refereed & Open Access International Journal - As per UGC Norms
(Fulfilled Suggests Parameters of UGC by IJMER)
Volume:15, Issue:7(2), July 2026
Scopus Review ID: A2B96D3ACF3FEA2A
Article Received: Reviewed: Accepted
Publisher: Sucharitha Publication, India
Online Copy of Article Publication Available: www.ijmer.in

[28] W. Xu, W. Liao, H. Zhou, L. Wang, K. Huang, P. Li, J. Yu, M-Type Ba-Hexaferrite Nanoplates with Exceptional Microwave Absorption Properties, ACS Appl. Electron. Mater. 6 (2024) 2759–2766. https://doi.org/10.1021/ACSAELM.4C00307.

[29] R. Verma, A. Chauhan, K.M. Batoo, R. Kumar, M. Hadi, E.H. Raslan, Structural, morphological, and optical properties of strontium doped lead-free BCZT ceramics, Ceram. Int. 47 (2021) 15442–15457. https://doi.org/10.1016/J.CERAMINT.2021.02.110.

[30] M. Rahman, M. Gafur, M.S.-Int.J.Innov.Res.Adv. Eng, undefined 2015, Impact of doping on structural, electronic and optical properties of cobalt ferrite prepared by solid-state reaction, Academia.Edu MA Rahman, MA Gafur, MR SarkerInt. J. Innov.

[31] S.T.A. Naqvi, S.K. Godara, B. Ray, S. Datar, C. Singh, Investigation of structural, hysteresis, and microwave dielectric/magnetic properties of Co-Zn doped M-type strontium hexaferrites for light-weight microwave absorber, SpringerSTA Naqvi, SK Godara, B Ray, S Datar, C SinghEmergent Materials, 2025•Springer 8 (2025) 3331–3353. https://doi.org/10.1007/S42247-025-01034-7.

[32] M. Ijaz, H. Ullah, B. Ali Al-Asbahi, M. Ullah Khan, Z. Abbas, S. Ullah Asif, Co-precipitation method followed by ultrafast sonochemical synthesis of aluminium doped M type BaFe11.4-xAlxCo0.6O19 hexaferrites for various applications, J. Magn. Magn. Mater. 589 (2024) 171559. https://doi.org/10.1016/J.JMMM.2023.171559.

[33] D. Sharma, Rohit, V. Singh, A. Dogra, M. Singh, Aluminium and praseodymium doped M-type hexaferrites for electric vehicle applications, Ceram. Int. 50 (2024) 24815–24822. https://doi.org/10.1016/J.CERAMINT.2024.04.217.

[34] P. Maltoni, R.K. Dokala, P. Pramanik, R. Araujo, T. Edvinsson, S.A. Ivanov, B. Almqvist, G. Varvaro, A. Capobianchi, N. Yaacoub, C. Hervoches, A. Martinelli, R.C. Pullar, D. Peddis, R. Mathieu, Temperature dependent magnetic and structural properties of Al substituted nanostructured hexaferrites with large coercive fields, Acta Mater. 313 (2026) 122273. https://doi.org/10.1016/J.ACTAMAT.2026.122273.

[35] G. Albanese, M. Carbucicchio, A. Deriu, Temperature dependence of the sublattice magnetizations in Al- and Ga-substituted M-type hexagonal ferrites, Physica Status Solidi (a) 23 (1974) 351–358. https://doi.org/10.1002/PSSA.2210230202;REQUESTEDJOURNAL:JOURNAL:1521396X;WGROUP:STRING:PUBLICATION.

[36] S. Kumar, S. Supriya, L.K. Pradhan, R. Pandey, M. Kar, Simultaneous effect of crystal lattice and non magnetic substitution on magnetic properties of barium hexaferrite, AIP Conf. Proc. 1953 (2018). https://doi.org/10.1063/1.5033105/793405.

[37] C. Kittel, Introduction to Solid State Physics, Wiley,... - Google Scholar, (n.d.).